Article

Current Design of Mixed-Ligand Complexes of Magnesium(II): Synthesis, Crystal Structure, Thermal Properties and Biological Activity against *Mycolicibacterium Smegmatis* and *Bacillus Kochii*

Marina E. Nikiforova [1], Dmitriy S. Yambulatov [1], Yulia V. Nelyubina [2], Petr V. Primakov [2], Olga B. Bekker [3], Konstantin B. Majorov [4], Maxim A. Shmelev [1], Andrey V. Khoroshilov [1], Igor L. Eremenko [1,2] and Irina A. Lutsenko [1,*]

1   N.S. Kurnakov Institute of General and Inorganic Chemistry of the Russian Academy of Sciences, Leninsky Prosp. 31, 119991 GSP-1 Moscow, Russia; yambulatov@yandex.ru (D.S.Y.)
2   A.N. Nesmeyanov Institute of Organoelement Compounds, Russian Academy of Sciences, Vavilova Str. 28, 119991 Moscow, Russia; petrprimakov@gmail.com (P.V.P.)
3   N. I. Vavilov Institute of General Genetics of the Russian Academy of Sciences, Gubkina, 3, 119333 Moscow, Russia; obekker@yandex.ru
4   Central Research Institute of Tuberculosis, Yauzskaya all., 2, 107564 Moscow, Russia
*   Correspondence: irinalu05@rambler.ru; Fax: +7-(495)-952-1279

Abstract: The interaction of Mg^{2+} with 2-furoic acid (HFur) and oligopyridines, depending on the synthesis conditions, leads to the formation of mixed-ligand complexes $[Mg(H_2O)_4(phen)] \cdot 2HFur \cdot phen \cdot H_2O$ (**1**), $[Mg(NO_3)_2(phen)_2]$ (**2**) and $[Mg_3(Fur)_6(bpy)_2] \cdot 3CH_3CN$ (**3**); these structures were determined with an SC X-ray analysis. According to the X-ray diffraction data, in complex **1**, obtained in ambient conditions, the magnesium cation coordinated four water molecules and one phenanthroline fragment, while in complexes **2** and **3** (synthesized in an inert atmosphere), the ligand environment of the complexing agent was represented by neutral oligopyridine molecules and acid anions. The thermal behavior of **1** and **2** was studied using a simultaneous thermal analysis (STA). The in vitro biological activity of complexes **1–3** was studied in relation to the non-pathogenic *Mycolicibacterium smegmatis* and the virulent strain *Mycobacterium tuberculosis* $H_{37}Rv$.

Keywords: magnesium(II); 2-furoic acid; 1,10-phenanthroline; 2,2′-bypiridine; crystal structure; simultaneous thermal analysis; *Mycolicibacterium smegmatis*; Mycobacterium tuberculosis

1. Introduction

The chemistry of alkaline-earth metal complexes is among the actively developing areas of coordination chemistry [1–9]. However, complexation with Mg^{2+} ions often demonstrates quite different binding schemes than the corresponding compounds of IIA metals [10–13]. This effect is primarily due to differences in the charge/ionic radius ratio (Mg^{2+} 0.801, Ca^{2+} 0.987, Sr^{2+} 1.076 and Ba^{2+} 1.118 [14,15]). For example, when magnesium interacts with carboxylate anions, it often tends to be surrounded by water molecules rather than by COO^- anions. (This fact was additionally explained using quantum-chemical calculations [16].) In terms of practical importance, studies on the development of MOFs based on magnesium complexes have recently become increasingly important too (e.g., magnesium sites improve the emission intensity of organic ligands, thus making Mg MOFs good fluorescence sensors) [12,17]. On the other hand, magnesium is a vital biogenic element [18–20] that participates in important biochemical processes in living systems: it ensures the proper operation of muscle fibers, the transmission of nerve impulses and the normalization of blood pressure and sugar levels; has an antitoxic effect; etc. However, an analysis of the literature showed an almost complete lack of data about studies on

the biological activity of magnesium carboxylate complexes with N-donor ligands [21–24]. 2-Furoic acid was chosen as the biological active organic component [25–27], the pharmacophore fragment of which is the founder of a whole group of antimicrobial drugs such as furazolidone, furadonin, enterofuril, etc. [28–33]. S. Melnic et al. investigated the in vitro activity of triangular furoate cobalt-iron {Fe$_2$CoO} complexes against *Mycobacterium tuberculosis* H$_{37}$Rv [34] and determined that Fe(III) furoate compounds can be used to increase the content of iron in microorganisms, which can be used in the agricultural industry [35]. 1,10-Phenanthroline (phen) and 2,2′-bipyridine (bpy) are promising nitrogen-donor ligands, increasing the biological activity of metal complexes [36–42]. Our previous work showed the effectiveness of the combination of biogenic metals with HFur and various pyridines (phen, bpy, 4-phenilpyridine) in the suppression of the vital activity of both regular lines of mycobacteria [43,44] and the exhibition of antiproliferative activity [45].

Based on the above, the purpose of this study is to develop a methodology for the synthesis of Mg^{2+} complexes with 2-furoic anions and oligopyridines, such as phen and bpy; to determine the structure of complexes via a single-crystal X-ray diffraction analysis; to investigate their thermal properties; and to study their biological activity in vitro with respect to mycobacteria, namely, *Mycolicibacterium smegmatis* (non-pathogenic strain) and *Mycobacterium tuberculosis* H$_{37}$Rv (bacillus Kochii).

2. Materials and Methods

2.1. General Remarks

The new complex **1** was synthesized in air using distilled water and commercial ethanol (96%). Commercial chemicals, MgO (Acros Organics, 98%), Mg(NO$_3$)$_2$·6H$_2$O (Rushim, 99%), 2-furoic acid (Hfur) (Acros Organics, 98%), 1,10-phenanthroline (Aldrich, 99%) and 2,2′-bipyridine (Aldrich, 99%) were used as received.

All manipulations related to the synthesis of compounds **2** and **3** were accomplished in inert atmosphere. Acetonitrile was dried with P$_2$O$_5$, kept on the activated molecular sieves (4 Å) and replaced within the reaction zone via vacuum condensation with liquid nitrogen just before the synthesis. Anhydrous Mg(CH$_3$COO)$_2$ was synthesized via a reaction of MgO and glacial acetic acid, and the product was dried in vacuo at 160 °C for 24 h. After isolation from the solution, samples of **2** and **3** were stable at ambient conditions. In solution, it tends to adsorb water vapors—that is why an inert atmosphere should be applied during the synthesis.

An elemental analysis was performed on a Carlo Erba EA 1108 Series CHN Elemental Analyzer. The IR spectra of the compound were measured on a Perkin-Elmer Spectrum 65 FTIR spectrophotometer in the attenuated total reflection (ATR) mode in the 400–4000 cm^{-1} frequency range (Center of Collective Use of IGIC RAS).

The purity of compounds **1**–**3** was approved using PXRD (see the Supplementary Materials, Figures S5–S7). The powder patterns were measured on a Bruker D8 Advance diffractometer with a LynxEye detector in Bragg-Brentano geometry, with the sample dispersed thinly on a zero-background Si sample holder, at λ(CuKα) = 1.54060 Å, at a θ/θ scan with variable slits (irradiated length 20 mm) from 5° to 45° 2θ for (1 and 2) and 5° to 45° 2θ for 3, and at a step size of 0.02°. The obtained patterns were refined with the Rietveld method using TOPAS 4 software.

The thermal behavior of complexes **1** and **2** were studied using the simultaneous thermal analysis (STA) technique for parallel recording of TG (thermogravimetry) and DSC (differential scanning calorimetry) curves. The study was performed on an STA 449 F1 Jupiter® instrument («NETZSCH») in Al-crucibles under a lid with a hole to ensure a vapor pressure of 1 atm during the thermal decomposition of the samples. The rate of heating to 500 °C was 10 °C min^{-1} under an argon atmosphere (contents: Ar > 99.998%, O$_2$ < 0.0002%, N$_2$ < 0.001%, water vapor < 0.0003% and CH$_4$ < 0.0001%). The sample mass was in the range of 10.48–18.27 mg. The accuracy of temperature measurements was ±0.7 °C, and that of mass changes was ±1 × 10^{-2} mg.

2.2. Synthesis of [Mg(H₂O)₄(phen)]·2fur·phen·H₂O (1)

To a mixture of weighed portions of MgO (50 mg, 1.24 mmol) and Hfur (278 mg, 2.48 mmol), 20 mL of ethanol was added, and the mixtures was stirred while boiling (343 K) for 1 h in ambient condition. Phen (492 mg, 2.48 mmol) was added to the resulting suspension and stirred for another 15 min while boiling. The solution was filtered and left to slowly evaporate at room temperature. Square colorless crystals formed after 5 days and, when suitable for X-ray diffraction analysis, were separated from the mother liquor via decantation, washed with cold ethanol ($T \approx 278$ K) and dried in air. The yield of compound was 590 mg (68%). Anal. calc. $C_{34}H_{32}MgN_4O_{11}$:C, 58.59; H, 4.63; N, 8.04. Found: C, 58.53; H, 4.70; N, 8.11. FT-IR (ATR), ν/cm^{-1}:3519 w, 3395–2770 m, 1582 s, 1558 s, 1517 m, 1476 s, 1425 m, 1386 s, 1359 ws, 1346 s, 1219 m, 1185 s, 1139 m, 1103 m, 1085 w, 1078 m, 1008 s, 928 m, 882 m, 787 s, 757 s, 725 vs, 628 w, 600 m, 527 w, 473 w, 463 w, 446 w, 414 vs.

2.3. Synthesis of [Mg(NO₃)₂(phen)₂] (2)

Weighed portions of Mg(NO₃)₂·6H₂O (256 mg, 1.0 mmol) and phen (360 mg, 2.0 mmol) were heated with acetonitrile (10 mL) in a sealed vial via an oil bath at 403 K until complete dissolution of the starting reagents. Slow cooling ($T = 10$ K per hour) led to the formation of colorless cube-shaped single crystals suitable for X-ray diffraction. The yield of compound was 0.417 g (82%; counting per Mg). Anal. calc. $C_{24}H_{16}MgN_6O_6$:C 56.66, H 3.17, N 16.52. Found:C 56.61, H 3.11, N 16.47. FT-IR (ATR), ν/cm^{-1}:3063 w, 1980 w, 1625 w, 1580 m, 1520 m, 1496 w, 1462 m, 1426 s, 1411 m, 1352 m, 1335 s, 1303 s, 1224 m, 1210 m, 1191 m, 1142 m, 1103 m, 1093 m, 1057 s, 1027 s, 985 w, 865 m, 855 s, 842 s, 825 m, 783 m, 768 m, 724 vs, 641 m, 555 w, 509 w, 455 w, 441 m, 419 m.

2.4. Synthesis of [Mg₃(fur)₆(bpy)₂]·3CH₃CN (3)

Samples of Mg(CH₃COO)₂ (142 mg, 1.0 mmol), HFur (224 mg, 2.0 mmol) and bpy (156 mg, 1.0 mmol) were heated with acetonitrile (10 mL) in a sealed vial via an oil bath at 383 K until the solution became clear. Slow cooling (10 K per hour) led to the formation of colorless rhombic-shaped single crystals suitable for X-ray diffraction. The yield of the compound was 0.305 g (80%; counting per Mg). Anal. calc. $C_{54}H_{40}Mg_3N_7O_{18}$: C 56.50, H 3.51, N 8.54. Found: C 56.41, H 3.45, N 8.49. FT-IR (ATR), ν/cm^{-1}: 3121 w, 2251 w, 1717 m, 1614 m, 1597 m, 1573 m, 1549 m, 1475 s, 1419 s, 1401 s, 1372 m, 1320 w, 1251 w, 1229 m, 1197 m, 1174 m, 1157 w, 1143 w, 1118 w, 1076 m, 1059 w, 1043 w, 1011 m, 931 m, 884 m, 838 m, 788 s, 758 s, 739 m, 652 m, 617 m, 597 m, 572 w, 494 m.

2.5. X-ray Study

The X-ray diffraction data for **1** was collected at 100 K with a Bruker Quest D8 CMOS diffractometer, while those for **2** and **3** were collected at 120 K with a Bruker APEX2 DUO CCD diffractometer, using graphite monochromate Mo-Kα radiation ($\lambda = 0.71073$ Å). Using Olex2 [46], the structures were solved with the ShelXT structure solution program [47] using Intrinsic Phasing and refined with the XL refinement package [48] with Least Squares minimisation. The hydrogen atoms of water molecules in **1** were located via difference Fourier synthesis, the positions of the other hydrogen atoms were calculated and they were all refined in the isotropic approximation of the riding model. The **3** ring fragments of the three furoate anions were disordered over two positions each with the following occupancies: O3:O3A 0.254(11):0.746(11); O15:O15A 0.539(12):0.461(12) and O18:O18A 0.478(14):0.522(14). The crystallographic parameters and the refinement statistics are given in Table 1. CCDC 2,245,826, 2,245,827 and 2,245,828 contain the supplementary crystallographic data for **1**, **2** and **3**, respectively. These data can be obtained free of charge from the Cambridge Crystallographic Data Centre http://www.ccdc.cam.ac.uk, accessed on 3 May 2023.

Table 1. Crystallographic parameters and structure refinement statistics for complexes **1**–**3**.

Compound	1	2	3
Empirical formula	$C_{34}H_{32}MgN_4O_{11}$	$C_{24}H_{16}MgN_6O_6$	$C_{56}H_{43}Mg_3N_7O_{18}$
Formula weight	696.94	508.74	1174.90
T (K)	100	120	120
Crystal system	orthorhombic	triclinic	triclinic
Space group	$Pna2_1$	P-1	P-1
a (Å)	13.9526(4)	7.9821(4)	12.2596(6)
b (Å)	22.5521(7)	11.0467(6)	13.6771(7)
c (Å)	10.2641(3)	13.1919(7)	17.5930(11)
α (deg)	90	80.1010(10)	84.945(2)
β (deg)	90	82.6730(10)	69.6460(10)
γ (deg)	90	73.2120(10)	89.6010(10)
V (Å^3)	3229.71(17)	1093.31(10)	2754.1(3)
Z	4	2	2
D_{calc} (g·cm^{-3})	1.433	1.545	1.417
μ (mm^{-1})	0.125	0.140	0.137
$F(000)$	1456	534	1216
Reflections measured	41,230	11,361	32,091
Independent reflections	6354	5761	13,293
R_{int}	0.0377	0.0224	0.0447
R_1 (all data)	0.0390	0.0536	0.0881
wR_2 (all data)	0.0957	0.1044	0.1284
R_1 ($I > 2\sigma(I)$)	0.0349	0.0404	0.0472
wR_2 ($I > 2\sigma(I)$)	0.0920	0.0962	0.1088
GooF	1.020	1.053	1.012
$\Delta\rho_{max}/\rho_{min}$ (e/Å^3)	0.414/−0.264	0.373/−0.250	0.586/−0.335

2.6. Antimycobacterial Activity **1**–**3**

2.6.1. Biological Activity against *Mycolicibacterium smegmatis* mc^2 155

To determine the biological activity of substances **1**–**3** possessing antiproliferative properties in the *M. smegmatis* test system, the paper disk method was used. The technique involved determining the size of the zone of inhibition of the growth of the strain seeded as a lawn on an agar medium, around paper disks containing the compound in various concentrations. The bacteria washed off Petri dishes with Trypton-soy agar M-290 medium (Himedia, city, country) were grown overnight in Lemco-TW liquid medium (Lab Lemco' Powder 5 gL^{-1} (Oxoid), Peptone special 5 gL^{-1} (Oxoid), NaCl 5 gL^{-1} and Tween-80) at +37 °C until the average logarithmic growth phase at optical density OD600 = 1.5 and then mixed with molten agar medium M-290 in a ratio of 1:9:10 (culture:Lemco-TW:M-290), and the resulting mixture was poured as a top layer onto Petri dishes, 5 mL per dish, with an already solidified M-290 agar medium. After the agar in the top layer solidified, paper disks soaked with a solution of the test substance were placed on the plate surface [49]. The culture was incubated for 24 h at +37 °C. The diameter of the zone of inhibition of *M. smegmatis mc^2 155* growth around the paper disk impregnated with the compound was determined. The MIC (minimum inhibiting concentration) was taken as the concentration of the compound where the zone of growth inhibition was the smallest.

2.6.2. Biological Activity against *Mycobacterium tuberculosis* H$_{37}$Rv

M. tuberculosis strain H$_{37}$Rv, sub-strain Pasteur from the collection of the Central Institute for Tuberculosis (Moscow, Russia), was maintained and prepared for in vitro studies exactly as described previously [50]. Briefly, 50 µL of a thawed 108 CFU/mL aliquot was added to 30 mL of a Dubos broth base (BD) supplemented with 0.5% fatty acid-poor BSA (Calbiochem) and incubated for 2 weeks at 37 °C. The resulting suspension was washed two times with Ca- and Mg-free PBS containing 0.2 mM EDTA and 0.025% Tween 80 (3000 g, 20 min, 4 °C), re-suspended in PBS with 0.025% Tween 80 and filtered

through a 5 µm pore-size filter (Millipore) to remove clumps. To estimate the CFU content in the filtrate, 20 µL from each 5-fold serial dilution was plated onto the Dubos agar (BD), and the total number of micro-colonies within the spot visible on the air-dried agar was calculated under an inverted microscope (200× magnification) after being cultured for 3 days at 37 °C. The bulk of the filtered culture was stored at 4 °C, and it was found that no change in the CFU content occurred during this storage period. To assess the direct effect of chemicals on *M. tuberculosis* $H_{37}Rv$ (Pasteur) and to determine the minimum inhibiting concentration (MIC) of the compounds, the serial dilution method was used with cultivation of mycobacteria in Dubos broth at 37 °C [51]. The growth of mycobacteria in the presence of various concentrations of the compounds being tested was assessed via the presence or absence of a visible sediment of mycobacteria at the bottom of round-bottom wells of a 96-well plate on the 13th day after the compounds had been added. The minimum inhibiting concentration (MIC 100%) was expressed as a range of concentrations of the test compound, where the upper limit of the range is the minimum concentration from the set of tested concentrations with no growth of mycobacteria and the lower limit is the maximum concentration of those tested with mycobacteria growth. To analyze the cytotoxicity of compounds for murine peritoneal macrophages, the CytoTox 96 kit (Promega) was used, and cytotoxicity was assessed via the release of the cytosolic marker of macrophages, the lactate dehydrogenase (LDH) enzyme, which appears in the supernatants of macrophage cultures as a result of macrophage lysis, into the culture medium. The specific lysis induced by the test compounds was calculated according to the manufacturer's recommendation. The experiment was carried out in triplicate.

3. Results and Discussion
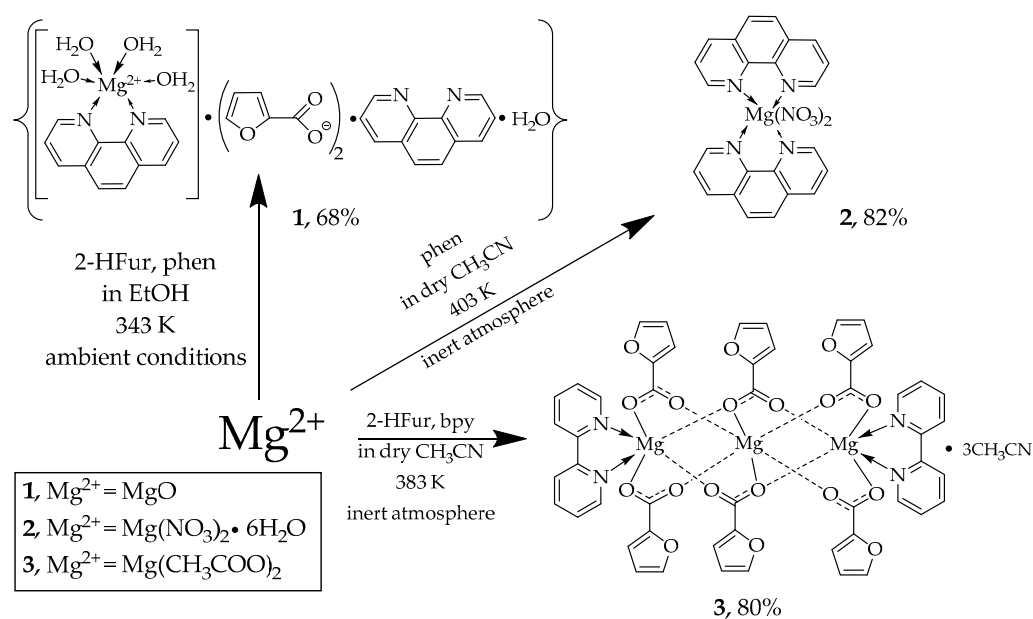
3.1. Synthesis of Compounds **1**–**3**

As a result of the reaction of MgO with HFur in ethanol in air, a suspension was first obtained, which, when phen was added and kept at 343 K with constant stirring, turned into a true solution. The resulting complex **1** contained four coordinated water molecules.

Despite the fact that the magnesium ion has a stable oxidation state of 2+, we had to synthesize complexes **2** and **3** in an inert atmosphere in dried solvents using the standard Schlenk technique and low-pressure sealed glass ampoules. Trying to synthesize complexes **2** and **3** in air, we obtained a mixture of products that could not be isolated in an individual state and that was characterized using physicochemical methods of analysis. We assume that the reason for this may be the high oxophilicity of the magnesium ion. A mixture of products can be attributed to complexes with different numbers of water molecules coordinated to the magnesium ion.

In Scheme 1 below, It can be seen the routes of synthesis compounds **1**–**3**.

3.2. Single Crystal X-ray Structures of **1**–**3**

The structures of **1**–**3** were confirmed via X-ray diffraction. According to the obtained data, complex **1** crystallizes in the orthorhombic space group *Pna2₁* as a solvate with lattice molecules of phenanthroline and water (Figure 1, top; Table 2). A pseudo-octahedral coordination environment of the metal ion, as gauged using continuous symmetry measures [52], consists of two nitrogen atoms of the phenanthroline ligand and four coordinated water molecules. The latter form hydrogen bonds with the two outer-sphere anions and lattice phenanthroline and water molecules (Table 3) to assemble the above species into hydrogen-bonded chains along the crystallographic axis *a*. Those are additionally stabilized via parallel-displaced stacking interactions between the aromatic cores of the coordinated and free phenanthroline molecules (Figure 1, bottom); the appropriate interplane angles are 3.55(3)–5.09(3)°, and the inter-centroid and shift distances are 3.8868(12)–4.1163(12) and 1.638(2)–2.4407(18) Å, respectively.
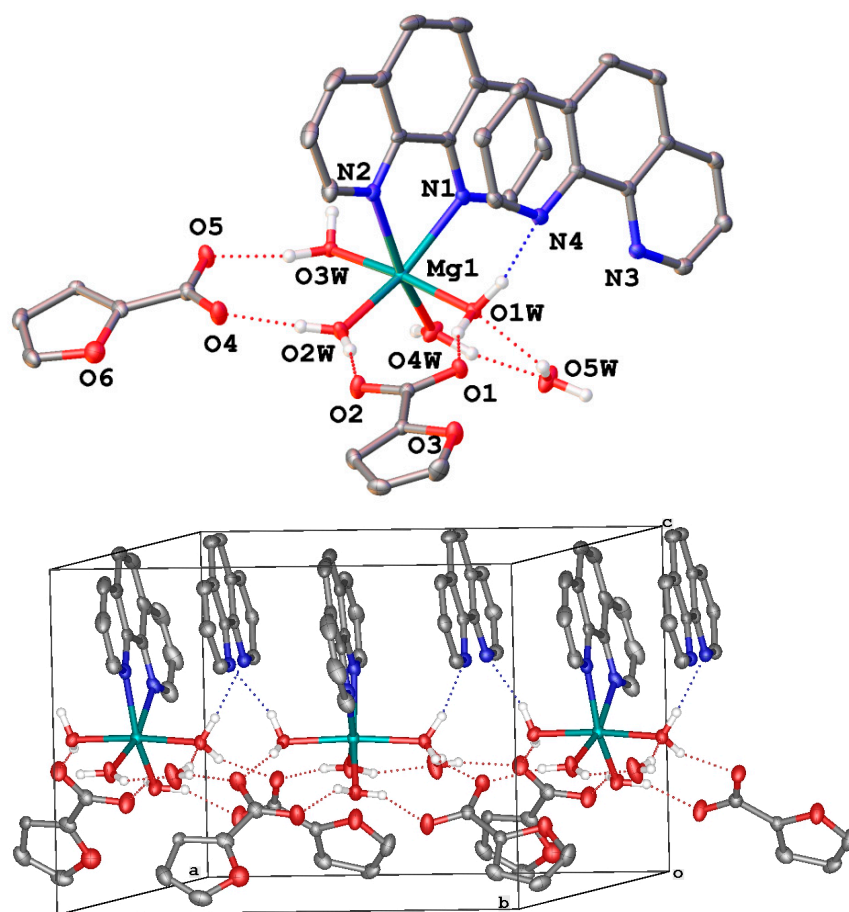
Scheme 1. Synthesis of complexes **1–3**.

Figure 1. A general view of **1** (**top**) and a fragment of its crystal packing illustrating the formation of hydrogen-bonded chains (**bottom**). Hereinafter, hydrogen atoms except those of water molecules are omitted, non-hydrogen atoms are shown as thermal ellipsoids (*p* = 30%), labels are given only for the heteroatoms in an asymmetric part of the unit cell, dotted lines stand for hydrogen bonds and aromatic fragments involved in stacking interactions are highlighted in pink.

Table 2. Main geometric parameters and continuous symmetry measures [a] as obtained from X-ray diffraction for **1**–**3**.

Parameter	1	2	3
	Bond, Å		
Mg−O(fur)	–	–	1.9980(15)–2.2038(15)
Mg−O(H$_2$O)	2.008(2)–2.117(2)	–	–
Mg−O(NO$_3$)	–	2.0442(11), 2.0311(11)	–
Mg−N	2.224(3), 2.257(3)	2.1966(12)–2.2148(12)	2.1537(18)–2.2101(18)
	Angle, °		
O-Mg-O	86.71(9)–174.03(10)	90.98(5)	88.31(5)–180.0
N-Mg-O	86.85(9)–164.78(11)	87.72(5)–168.88(5)	83.89(6)–179.03(7)
N-Mg-N	73.69(10)	75.63(5)–163.09(5)	74.61(7), 75.23(7)
	Continuous symmetry measures		
S(OC)	1.164	1.573	0.029, 2.618 [0.007, 2.700] [b]
S(TPR)	10.933	10.605	16.376, 12.410 [16.655, 11.107] [b]

[a] S(OC) and S(TPR) are octahedral and trigonal-prismatic symmetry measures, respectively. [b] The values are given for the central and peripheral metal ion, respectively; those for the second symmetry-independent molecule of the complex are given in brackets.

Table 3. Parameters of hydrogen bonds in the crystal of **1**.

D	H	A	*d*(D–H), Å	*d*(H–A), Å	*d*(D–A), Å	D-H-A, °
O3W	H3WA	N3 [1]	0.86	1.99	2.820(3)	160.7
O3W	H3WB	O5	0.94	1.82	2.755(3)	169.7
O1W	H1WA	N4	0.94	1.84	2.768(3)	166.1
O1W	H1WB	O1	0.95	1.83	2.725(3)	157.0
O2W	H2WA	O2	0.88	1.77	2.644(3)	172.5
O2W	H2WB	O4	0.86	1.81	2.657(3)	173.9
O4W	H4WA	O3 [1]	0.95	2.45	2.929(3)	111.6
O4W	H4WA	O5W	0.95	1.87	2.761(3)	155.5
O4W	H4WB	O1 [1]	0.97	1.80	2.758(3)	168.5
O5W	H5WA	O1W	0.92	2.20	2.930(3)	135.3
O5W	H5WB	O5 [2]	0.88	1.90	2.754(3)	163.5

[1] $1/2 + x$, $1/2 − y$, $+z$; [2] $−1/2 + x$, $1/2 − y$, $+z$.

Complex **2** crystallizes in the triclinic space group *P*-1 with no lattice solvents. The magnesium(II) ion coordinates four nitrogen atoms of the two phenanthroline ligands and two oxygen atoms of two nitrate anions in the vertices of a slightly more distorted octahedron (Figure 2, top; Table 2). The angle between the planes of the phenanthroline ligands is 99.16(2)°, and that between the nitrate anions is 90.11(17)°. Parallel-displaced stacking interactions between the phenanthroline ligands (with the interplane angle of 0.0° and the inter-centroid and shift distances of 4.4832(8)–5.4058(9) and 2.9760(14)–4.2455(11) Å, respectively) assemble the molecules of the complex **2** into layers along the diagonal of the crystallographic plane *b0c* (Figure 2, bottom).
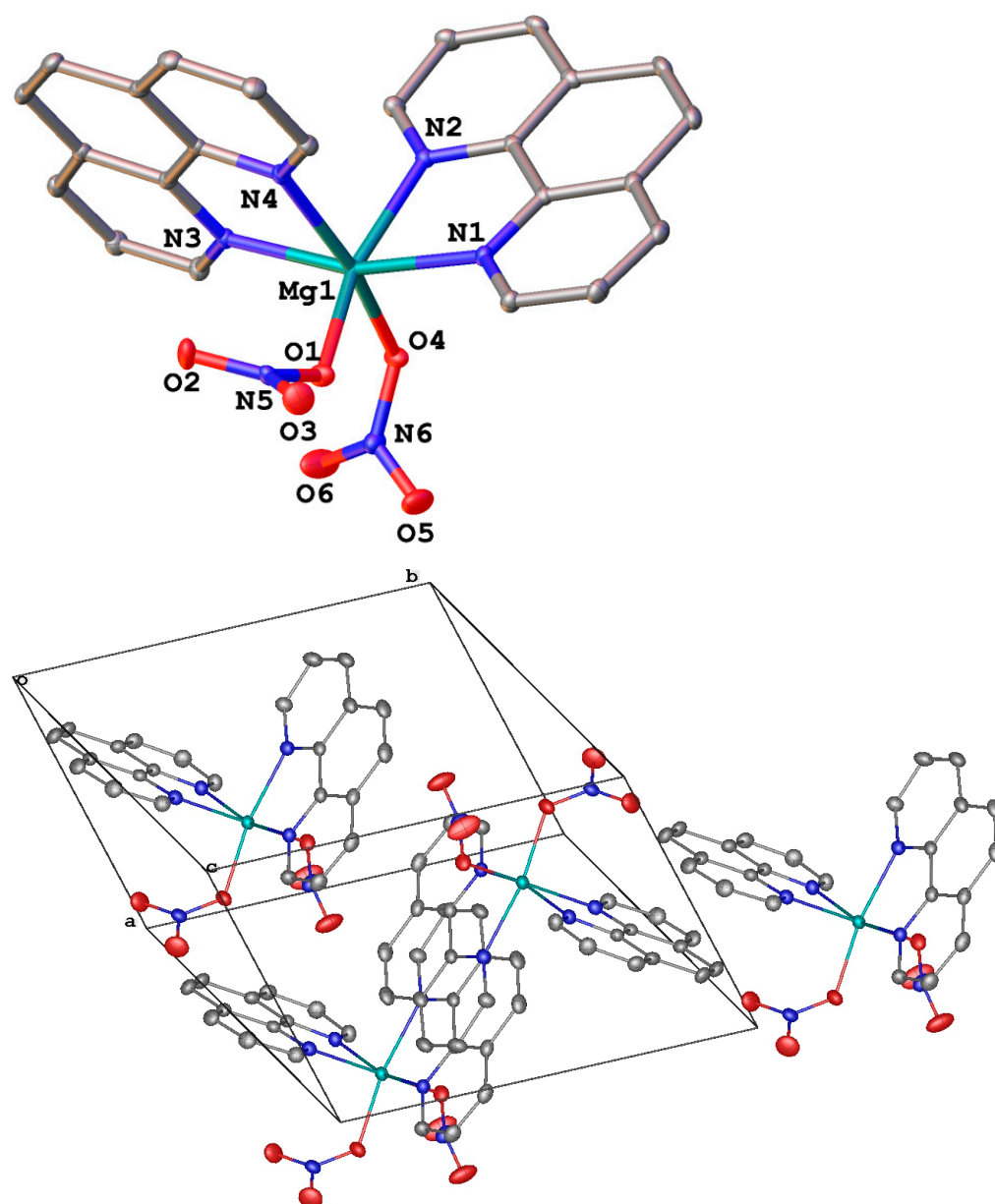
Figure 2. A general view of **2** (**top**) and a fragment of its crystal packing illustrating the formation of layers via stacking interactions (**bottom**).

Complex **3** crystallizes in the triclinic space group *P*-1 with three molecules of solvent acetonitrile and two symmetry-independent molecules of the target complex both occupying the inversion center that coincides with the position of the central magnesium(II) ion. The latter coordinates six oxygen atoms of the six bridging anions in the vertices of an almost ideal octahedral (Figure 3, top; Table 2) as gauged by the near-zero values of the appropriate symmetry measure [52]. Two of these bridging anions also act as a bidentate ligand to the two peripheral magnesium(II) ions each coordinating four oxygen atoms of the three anions and two nitrogen atoms of the bipyridine ligand in its pseudo-octahedral coordination environment. The symmetry-independent molecules of the complex are held together via parallel-displaced stacking interactions between the bipyridine ligands and one of the three symmetry-independent anions (with the interplane angle of 4.64(8)–6.4(5)° and the inter-centroid and shift distances of 3.6851(12)–3.901(6) and 1.4845(17)–2.160(5) Å, respectively) to produce chains along the volumetric diagonal of the unit cell (Figure 3, bottom). These chains are assembled into layers along the diagonal of the

crystallographic plane *a0c* (Figure 3, bottom) via parallel-displaced stacking interactions between the bipyridine ligands and their symmetry-equivalent counterparts; the appropriate interplane angle is 0.0°, and the inter-centroid and shift distances are 3.7919(14)–3.9640(14) and 1.450(3)–1.753(3) Å, respectively.
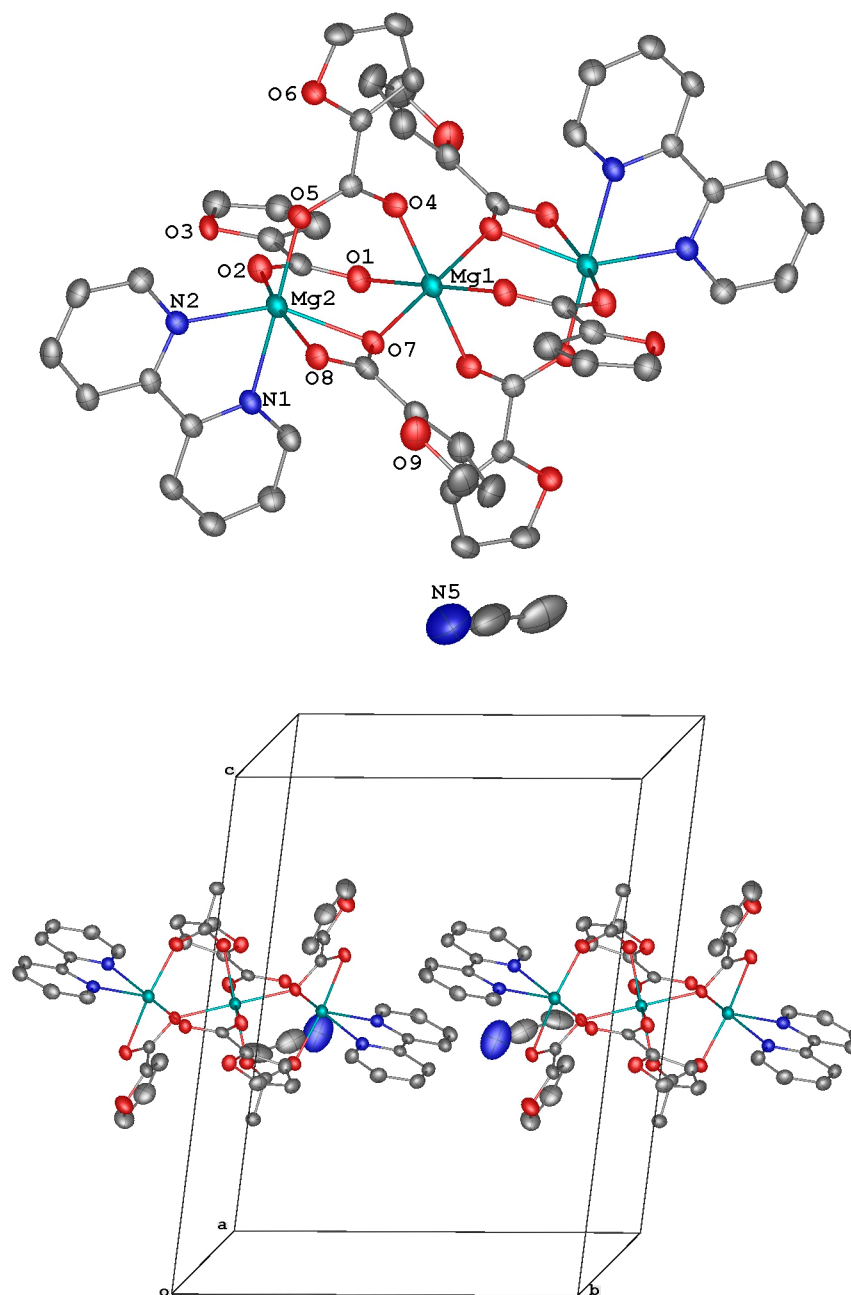

Figure 3. A general view of **3**. Minor components of the disordered anions, the second symmetry-independent molecule of the complex, which also occupies a special position (the inversion center that coincides with the location of the ion Mg(1), are not shown).

3.3. Thermal Properties of **1** and **2**

Thermal behavior of complexes **1** and **2** was studied using the STA method under argon with simultaneous TG and DSC recording (Figure 4 and Table 4). The difference in the structures of the outer and inner coordination spheres of the complexes led to a fundamentally different nature of the thermal destruction of these complexes. Complex **1** is stable up to 92 °C. The thermal destruction of complex **1** proceeds stepwise. The first

step is associated with the elimination of outer sphere and coordinated water molecules ($m_{\text{exp./calc}}$ = 12.3/12.9%) (Figure 4a, **1**; Table 4).
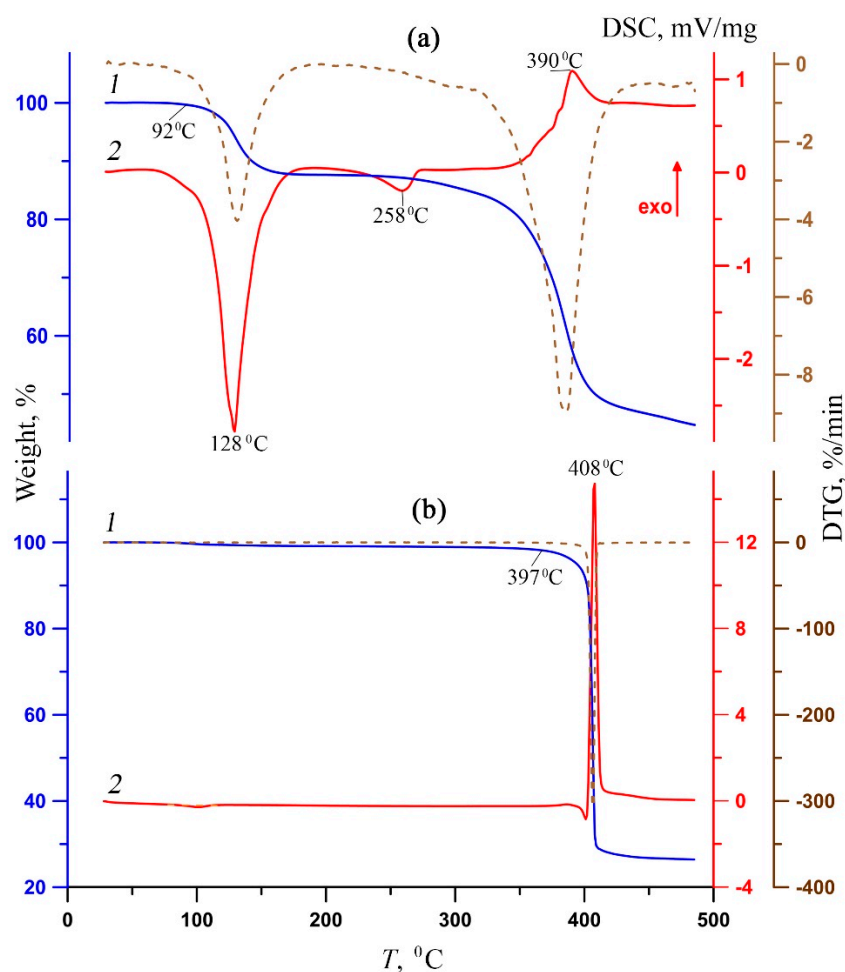

Figure 4. TG (1, blue), DSC (2, red) and DTG (dotted brown) curves of complexes **1** (**a**) and **2** (**b**).

Table 4. Thermal analysis data for complexes **1** and **2** (inert atmosphere).

Complex	Stage/ΔT, °C	Δm (TG), %	$T_{\text{endo/exo}}$, °C	m_{fin}, %
1	1 (92–170)	12.3	128 ± 0.7	44.7
	2 (170–485)	41.1	389.8 ± 0.7	
2	1 (397–425)	71.9	407.5 ± 0.7	26.4

The process on the DSC curve (Figure 4a, **2**) corresponds to an intense broadened endothermic effect, which is characteristic of dehydration processes [53,54]. The subsequent behavior of the sample indicates its thermal stability up to 310 °C. (It is possible that the elimination of coordinated water molecules and, as a result, the release of vacant coordination possibilities of magnesium, led to the coordination of another phen molecule, which was previously in the outer sphere.) A weak Endo effect on the DSC curve with an extremum at 258 °C mean structural changes. The second stage is associated with the thermal destruction of the organic part (decarboxylation and deamination). In this case, the total weight loss on the TG curve is approximately 41%, and on the DSC curve, there is an exothermic effect with an extremum of 390 °C (Figure 4a). In contrast to **1**, complex **2** is characterized by extreme thermal stability (up to 397 °C; Figure 4b, *1*; Table 4), and the entire thermolysis process proceeds in a narrow temperature range (27 °C). At the same time, the DSC curve (Figure 4b, 2) shows a single narrow intense exothermic

effect corresponding to the sublimation of the thermolysis product. The high final weight of the thermolyzed sample **1**, almost 45%, indicates the incompleteness of the thermal decomposition process at 500 °C, while for **2**, the residual weight is two times less (27%).

*3.4. Antimycobacterial Activity of **1**–**3** against M. smegmatis and M. tuberculosis $H_{37}Rv$*

The antibacterial activity of compounds **1**–**3** was determined in vitro against a non-pathogenic *M. smegmatis* strain. It is known that the resistance of mycobacteria to chemotherapeutic agents is due to the low permeability of the mycobacterial cell wall that has an unusual structure. *M. smegmatis* are fast-growing non-pathogenic bacteria and are therefore used as organisms simulating the slow-growing *M. tuberculosis* bacteria, as well as for primary screening of anti-tuberculosis drugs [49]. The *M. smegmatis* test system exhibits a higher degree of resistance to antibiotics and antituberculosis agents than *M. tuberculosis*; therefore, the selection criterion is a compound concentration of <100 nmol/disc, in contrast to *M. tuberculosis* (MIC < 2 µg/mL) [55]. All the results obtained for in vitro bioactivity of the studied compounds were compared with the activity of rifampicin (Rif), i.e., the first-line drug for tuberculosis treatment under these experimental conditions. The concentration of the compound, at which the minimum visible zone of growth inhibition is observed, is considered as the MIC (minimum inhibitory concentration, nmol/disc). The results of antibacterial activity in the *M. smegmatis* mc^2 155 test system and its variation over time for compounds **1**–**3** are shown in Table 5. According to Table 5, the value of MIC **1** corresponds to the value of Rif and indicates a high biological activity against a non-pathogenic strain of *M. smegmatis*. Despite the fact that complex **2** contains two phen fragments, its activity is five times lower than that of **1**. In general, in the process of studying the antimycobacterial activity of the complexes, it was noted that compounds containing oligopyridine fragments always exhibit greater bioactivity than those with monopyridine fragments [56]. In contrast to **1** and **2**, compound **3** exhibits no valuable bioactivity—the MIC is forty times lower than that of Rif. The MIC values for free ligands (Table 5) are, on the one hand, significantly lower than those for complexes; on the other hand, their individual effectiveness is low, as evidenced by the "zero" zone of inhibition, i.e., the action of the free ligand on the strain ends within the first day (unlike complexes).

Table 5. Results in vitro antibacterial activity of **1**–**3** against *M. smegmatis*.

Compound	MIC, nmol/Disk 24 h	Zone of Inhibition, mm		Ref
		24 h	120 h	
1	10	6.5 ± 0.2 *	6.3 ± 0.2 *	this work
2	20	7.5 ± 0.3	6.5 ± 0.3 **	this work
3	200	7.0 ± 0.5 *	6.1 ± 0.1 *	this work
[Cu(fur)$_2$(phen)]	5	7 ± 0.5 **	7 ± 0.5 **	[43]
[Cu$_2$(NO$_2$-fur)$_4$(bpy)$_2$]·H$_2$O	20	7.0 ± 0.0	6.9 ± 0.1 *	[56]
[Cu(fur)$_2$(neoc)(H$_2$O)]	25	6.7 ± 0.3	6.6 ± 0.1 **	[57]
[Cu(fur)$_2$(bpy)(H$_2$O)]	100	7.0 ± 0.5	7.0 ± 0.5 **	[44]
Hfur	1000	0	0	this work
bpy	500	0	0	this work
phen	50	7.5 ± 0.5	0	this work
neocuproine	100	6.5 ± 0.1	0	[57]
Rifampicin	6	7.2 ± 0.3 **	7.13 ± 0.35 **	this work

* *M. smegmatis* growth inhibition zone overgrows (bacteriostatic effect). ** The zone of growth inhibition of *M. smegmatis* is transparent; there is no weak background growth of the culture (bactericidal effect). 0—There is no culture growth zone.

For complexes **1** and **2**, which showed the highest activity against the *M. smegmatis* strain (which is a model in relation to *M. tuberculosis*), an assessment of bioefficiency was determined. The specific pharmacological activity of complexes **1** and **2** were determined in vitro on the model system (MBT $H_{37}Rv$). The values of MIC for **1** and **2** determined with

respect to the reference (museum) strains *M. tuberculosis* H$_{37}$Rv (Table 6) are comparable with those of Isoniazid (INH 0.1 μg/mL), a first-line antituberculosis drug.

Table 6. The results of anti-tuberculosis activity of **1** and **2** against MBT H$_{37}$Rv.

Complex	MIC for Free MBT H$_{37}$Rv(μg/mL) *	MIC for Free MBT H$_{37}$Rv(μg/mL) **	% of Specific Lysis of Macrophages			IC$_{50}$, μg/mL	SI
			20 (μg/mL)	10 (μg/mL)	5 (μg/mL)		
1	1.48–4.44	2.53–3.38	-	-	-	-	-
2	1.48–4.44	1.42–1.90	68.4 ± 8.5	18.5 ± 3.6	9.2 ± 4.7	10	~6

* MIC range at day 14 after addition of complexes (three-fold dilution); ** MIC range at day 14 after addition of complexes (one-threefold dilution).

After the screening of complexes **1** and **2** against the *M. tuberculosis* H$_{37}$Rv reference strain, both complexes were tested at narrower intervals. According to the results of the second screening, **2** passed for further tests, showing values less than 2 μg/mL. Estimation of the cytotoxicity of **2** for murine peritoneal macrophages was based on the release into the culture medium of the cytosolic marker of macrophages, the lactate dehydrogenase (LDH) enzyme, which appears in the supernatants of macrophage cultures due to macrophage lysis. The percentage of specific lysis at concentrations of 5–20 μg/L was 9–68%, respectively, which is an indicator of the high activity of the test compound (Table 6). The selectivity index (SI) of complex **2**, which is defined as the ratio of IC$_{50}$ (the concentration of the compound that results in the 50% macrophage lysis) and the MIC of this compound with respect to *M. tuberculosis* H$_{37}$Rv, is 6 (Table 6). Thus, the data obtained (SI < 10) do not exclude the possibility of using the studied compound to create anti-tuberculosis drugs at correctly selected concentrations.

4. Conclusions

In summary, new crystalline mixed-ligand mono- and trinuclear complexes of Mg(II) with oligopyridines have been obtained. According to the X-ray diffraction data, in all compounds, the magnesium cation is in an octahedral environment {MgN$_2$O$_4$}, {MgN$_4$O$_2$}, {MgO$_6$}, realizing the coordination number 6. Additional stabilization of the supramolecular level is carried out with the help of hydrogen bonds (**1**) and π-stacking interactions (**1–3**). These interactions also determine the high thermal stability **1** and **2** according to STA data. Complexes **1** and **2** exhibit high antimycobacterial activity in vitro against *M. smegmatis and M. tuberculosis*.

Conflicts of Interest: The authors declare that they have no known competing financial interest or personal relationships that could have appeared to influence the work reported in this paper.

Sample Availability: Samples of compounds **1**–**3** are available from the authors.

References

1. Dimé, A.K.D.; Cattey, H.; Lucas, D.; Devillers, C.H. Electrosynthesis and X-Ray Crystallographic Structure of ZnII Meso-Triaryltriphenylphosphonium Porphyrin and Structural Comparison with MgII Meso-Triphenylphosphonium Porphine. *Eur. J. Inorg. Chem.* **2018**, *2018*, 4834–4841. [CrossRef]
2. Bhattacharjee, J.; Harinath, A.; Sarkar, A.; Panda, T.K. Polymerization of ε-Caprolactam to Nylon-6 Catalyzed by Barium σ-Borane Complex under Mild Condition. *ChemCatChem* **2019**, *11*, 3366–3370. [CrossRef]
3. Nandi, S.; De Luna, P.; Maity, R.; Chakraborty, D.; Daff, T.; Burns, T.; Woo, T.K.; Vaidhyanathan, R. Imparting Gas Selective and Pressure Dependent Porosity into a Non-Porous Solid via Coordination Flexibility. *Mater. Horizons* **2019**, *6*, 1883–1891. [CrossRef]
4. Paluchowska, B.; Maurin, J.K.; Leciejewicz, J. Direct and Outer-Sphere Coordination of the Magnesium Ions in the Crystal Structures of Complexes with 2-Furancarboxylic Acid (I) and 3-Furancarboxylic Acid (II). *J. Chem. Crystallogr.* **1997**, *27*, 177–182. [CrossRef]
5. Yang, J.; Yin, X.; Wu, L.; Wu, J.; Zhang, J.; Gozin, M. Alkaline and Earth Alkaline Energetic Materials Based on a Versatile and Multifunctional 1-Aminotetrazol-5-One Ligand. *Inorg. Chem.* **2018**, *57*, 15105–15111. [CrossRef]
6. Wan, K.-K.; Yu, J.-H.; Yang, Q.-F.; Xu, J.-Q. 5,5′-(1,4-Dioxo-1,2,3,4-Tetrahydrophthalazine-6,7-Diyl)Bis(Oxy)Diisophthalate-Based Coordination Polymers and Their TNP Sensing Ability. *Eur. J. Inorg. Chem.* **2019**, *2019*, 3094–3102. [CrossRef]
7. Roueindeji, H.; Ratsifitahina, A.; Roisnel, T.; Dorcet, V.; Kahlal, S.; Saillard, J.-Y.; Carpentier, J.-F.; Sarazin, Y. Metal···F−C Bonding in Low-Coordinate Alkaline Earth Fluoroarylamides. *Chem.–A Eur. J.* **2019**, *25*, 8854–8864. [CrossRef]
8. Moskalev, M.V.; Skatova, A.A.; Razborov, D.A.; Bazanov, A.A.; Bazyakina, N.L.; Sokolov, V.G.; Fedushkin, I.L. Magnesium and Calcium Complexes of ArBIG-Bian and Their Reactivity towards CO$_2$ (ArBIG-Bian=1,2-Bis[(2,6-Dibenzhydryl-4-Methylphenyl)Imino]Acenaphthene). *Eur. J. Inorg. Chem.* **2021**, *2021*, 1890–1896. [CrossRef]
9. Bazyakina, N.L.; Makarov, V.M.; Ketkov, S.Y.; Bogomyakov, A.S.; Rumyantcev, R.V.; Ovcharenko, V.I.; Fedushkin, I.L. Metal–Organic Frameworks Derived from Calcium and Strontium Complexes of a Redox-Active Ligand. *Inorg. Chem.* **2021**, *60*, 3238–3248. [CrossRef]
10. Anker, M.D.; Kefalidis, C.E.; Yang, Y.; Fang, J.; Hill, M.S.; Mahon, M.F.; Maron, L. Alkaline Earth-Centered CO Homologation, Reduction, and Amine Carbonylation. *J. Am. Chem. Soc.* **2017**, *139*, 10036–10054. [CrossRef]
11. Yuan, N.; Zhang, M.; Cai, H.; Liu, Z.; Zhao, R. Two New Coordination Polymers Constructed from S-Block Alkaline Earth Metals and 2-hydroxylnicotinic Acid. *Inorg. Chem. Commun.* **2019**, *101*, 130–134. [CrossRef]
12. Li, N.; Zhao, Z.; Yu, C.; Wu, B.; Bian, Z.; Zhang, W.-X.; Xi, Z. Alkaline-Earth Metallacyclic Complexes Bearing a Diborane-Bridged Tetraamide Ligand: Synthesis, Structure and Fluorescence Property. *Dalton Trans.* **2019**, *48*, 9067–9071. [CrossRef] [PubMed]
13. Fedushkin Igor, L.; Chudakova Valentina, A.; Hummert Markus, S.H. Electron Release and Proton Acceptance Reactions of (Dpp-BIAN)Mg(THF)$_3$. *Zeitschrift für Naturforsch.* **2007**, *63*, 161–168. [CrossRef]
14. Brent Cole, L.; Holt, E.M. Alkali and Alkaline Earth Complexation to Derivatives of Salicylic Acid: [Calcium(p-Aminosalicylate)(Acetate)(H$_2$O)] (H$_2$O), Magnesium(Salicylate)$_2$(H$_2$O)$_4$, Magnesium(p-Aminosalicylate)$_2$(H$_2$O)$_4$, Magnesium(2, 6-Pyridinedicarboxylate)-(H2O)$_3$(H$_2$O)$_2$ and Sodium(p-A. *Inorganica Chim. Acta* **1989**, *160*, 195–203. [CrossRef]
15. Prince, E. *Tables for X-ray Crystalography; International Union of Crystallography*; Kluwer Academic Publishers: Dordrecht, The Netherlands, 1995; ISBN 1402019009.
16. Gupta, M.P.; van Alsenoy, C.; Lenstra, A.T.H. A Note on Polarization Effects Around the Magnesium Cation. *Bull. des Sociétés Chim. Belges* **1985**, *94*, 161–162. [CrossRef]
17. Lei, X.-J.; Hou, X.-Y.; Li, S.-N.; Jiang, Y.-C.; Sun, G.-X.; Hu, M.-C.; Zhai, Q.-G. Design of High-Symmetrical Magnesium-Organic Frameworks with Acetate as Modulator and Their Fluorescence Sensing Performance. *Inorg. Chem.* **2018**, *57*, 14280–14289. [CrossRef]
18. Rogolino, D.; Carcelli, M.; Sechi, M.; Neamati, N. Viral Enzymes Containing Magnesium: Metal Binding as a Successful Strategy in Drug Design. *Coord. Chem. Rev.* **2012**, *256*, 3063–3086. [CrossRef]
19. Black, C.B.; Huang, H.-W.; Cowan, J.A. Biological Coordination Chemistry of Magnesium, Sodium, and Potassium Ions. Protein and Nucleotide Binding Sites. *Coord. Chem. Rev.* **1994**, *135–136*, 165–202. [CrossRef]
20. Williams, R.J.P. Tilden Lecture. The Biochemistry of Sodium, Potassium, Magnesium, and Calcium. *Q. Rev. Chem. Soc.* **1970**, *24*, 331–365. [CrossRef]
21. Dimitrov, G.; Kaloyanov, N.; Petrov, P.; Wesselinova, D. Antibacterial Activity of Novel Compounds Obtained on Interaction of 1, 10-Phenanthroline with Alkaline Earth Metal Ions, Palladium (II) and NaBF$_4$. *Comptes rendus l'Academie Bulg. des Sci.* **2008**, *61*, 595–602.

22. da Silva, D.F.; Amaral, J.C.; Carlos, R.M.; Ferreira, A.G.; Forim, M.R.; Fernandes, J.B.; Della Coletta Filho, H.; de Souza, A.A. Octahedral Ruthenium and Magnesium Naringenin 5-Alkoxide Complexes: NMR Analysis of Diastereoisomers and in-Vivo Antibacterial Activity against Xylella Fastidiosa. *Talanta* **2021**, *225*, 122040. [CrossRef] [PubMed]

23. Marchi, R.C.; Silva, E.S.; Santos, J.J.; Guiloski, I.C.; de Jesus, H.C.R.; de Aguiar, I.; Kock, F.V.C.; Venâncio, T.; da Silva, M.F.G.F.; Fernandes, J.B.; et al. Synthesis, Characterization, and Low-Toxicity Study of a Magnesium(II) Complex Containing an Isovanillate Group. *ACS Omega* **2020**, *5*, 3504–3512. [CrossRef] [PubMed]

24. Drevenšek, P.; Košmrlj, J.; Giester, G.; Skauge, T.; Sletten, E.; Sepčić, K.; Turel, I. X-ray Crystallographic, NMR and Antimicrobial Activity Studies of Magnesium Complexes of Fluoroquinolones – Racemic Ofloxacin and Its S-Form, Levofloxacin. *J. Inorg. Biochem.* **2006**, *100*, 1755–1763. [CrossRef] [PubMed]

25. Zhang, Y.; Zhang, Y. A Comprehensive Review of Furan in Foods: From Dietary Exposures and in Vivo Metabolism to Mitigation Measures. *Compr. Rev. Food Sci. Food Saf.* **2023**, *22*, 809–841. [CrossRef] [PubMed]

26. Panda, L.; Duarte-Sierra, A. Recent Advancements in Enhancing Antimicrobial Activity of Plant-Derived Polyphenols by Biochemical Means. *Horticulturae* **2022**, *8*, 401. [CrossRef]

27. Becerra, M.L.; Prieto, G.A.; Rendueles, M.; Diaz, M. Biological Transformations of Furanic Platform Molecules to Obtain Biomass-Derived Furans: A Review. *Biomass Convers. Biorefinery* **2022**. [CrossRef]

28. Yi-Chang, N.; Heflich, R.H.; Kadlubar, F.F.; Fu, P.P. Mutagenicity of Nitrofurans in Salmonella Typhimurium TA98, TA98NR and TA98/1,8-DNP6. *Mutat. Res. Lett.* **1987**, *192*, 15–22. [CrossRef]

29. Sharma, S.; Anand, N. Chapter 17 - Nitroheterocycles. In *Approaches to Design and Synthesis of Antiparasitic Drugs*; Sharma, S., Anand, N.B.T.-P.L., Eds.; Elsevier: Amsterdam, The Netherlands, 1997; Volume 25, pp. 421–438. ISBN 0165-7208.

30. Greenaway, J.C.; Fantel, A.G.; Juchau, M.R. On the Capacity of Nitroheterocyclic Compounds to Elicit an Unusual Axial Asymmetry in Cultured Rat Embryos. *Toxicol. Appl. Pharmacol.* **1986**, *82*, 307–315. [CrossRef]

31. Deng, F.; Dong, C.; Liu, Y. Characterization of the Interaction between Nitrofurazone and Human Serum Albumin by Spectroscopic and Molecular Modeling Methods. *Mol. Biosyst.* **2012**, *8*, 1446–1451. [CrossRef]

32. Nakamura, H.; Kawakami, T.; Niino, T.; Takahashi, Y.; Onodera, S. Chemical Fate and Changes in Mutagenic Activity of Antibiotics Nitrofurazone and Furazolidone during Aqueous Chlorination. *J. Toxicol. Sci.* **2008**, *33*, 621–629. [CrossRef]

33. Hooper, G.; Covarrubias, J.J.P. Clinical Use and Efficacy of Furacin: A Historical Perspective. *J. Int. Med. Res.* **1983**, *11*, 289–293. [CrossRef] [PubMed]

34. Melnic, S.; Prodius, D.; Stoeckli-Evans, H.; Shova, S.; Turta, C. Synthesis and Anti-Tuberculosis Activity of New Hetero(Mn, Co, Ni)Trinuclear Iron(III) Furoates. *Eur. J. Med. Chem.* **2010**, *45*, 1465–1469. [CrossRef] [PubMed]

35. Melnic, S.; Prodius, D.; Simmons, C.; Zosim, L.; Chiriac, T.; Bulimaga, V.; Rudic, V.; Turta, C. Biotechnological Application of Homo- and Heterotrinuclear Iron(III) Furoates for Cultivation of Iron-Enriched Spirulina. *Inorganica Chim. Acta* **2011**, *373*, 167–172. [CrossRef]

36. Viganor, L.; Howe, O.; McCarron, P.; McCann, M.; Devereux, M. The Antibacterial Activity of Metal Complexes Containing 1, 10-Phenanthroline: Potential as Alternative Therapeutics in the Era of Antibiotic Resistance. *Curr. Top. Med. Chem.* **2017**, *17*, 1280–1302. [CrossRef]

37. Abu Ali, H.; Fares, H.; Darawsheh, M.; Rappocciolo, E.; Akkawi, M.; Jaber, S. Synthesis, Characterization and Biological Activity of New Mixed Ligand Complexes of Zn(II) Naproxen with Nitrogen Based Ligands. *Eur. J. Med. Chem.* **2015**, *89*, 67–76. [CrossRef]

38. Hachey, A.C.; Havrylyuk, D.; Glazer, E.C. Biological Activities of Polypyridyl-Type Ligands: Implications for Bioinorganic Chemistry and Light-Activated Metal Complexes. *Curr. Opin. Chem. Biol.* **2021**, *61*, 191–202. [CrossRef]

39. McCann, M.; Kellett, A.; Kavanagh, K.; Devereux, M.; Santos, A.L.S. Deciphering the Antimicrobial Activity of Phenanthroline Chelators. *Curr. Med. Chem.* **2012**, *19*, 2703–2714. [CrossRef]

40. Li, F.; Collins, J.G.; Keene, F.R. Ruthenium Complexes as Antimicrobial Agents. *Chem. Soc. Rev.* **2015**, *44*, 2529–2542. [CrossRef]

41. Ermakova, E.A.; Golubeva, Y.A.; Smirnova, K.S.; Klyushova, L.S.; Berezin, A.S.; Fetisov, L.N.; Svyatogorova, A.E.; Andros, N.O.; Zubenko, A.A.; Lider, E. V Cytotoxic Mixed-Ligand Copper(Ii) Complexes with 1H-Tetrazole-5-Acetic Acid and Oligopyridine Derivatives. *New J. Chem.* **2023**, *47*, 9472–9482. [CrossRef]

42. Ermakova, E.A.; Golubeva, J.A.; Smirnova, K.S.; Klyushova, L.S.; Eltsov, I.V.; Zubenko, A.A.; Fetisov, L.N.; Svyatogorova, A.E.; Lider, E. V Bioactive Mixed-Ligand Zinc(II) Complexes with 1H-Tetrazole-5-Acetic Acid and Oligopyridine Derivatives. *Polyhedron* **2023**, *230*, 116213. [CrossRef]

43. Lutsenko, I.A.; Baravikov, D.E.; Kiskin, M.A.; Nelyubina, Y.V.; Primakov, P.V.; Bekker, O.B.; Khoroshilov, A.V.; Sidorov, A.A.; Eremenko, I.L. Bioisostere Modifications of Cu^{2+} and Zn^{2+} with Pyromucic Acid Anions and N-Donors: Synthesis, Structures, Thermal Properties, and Biological Activity. *Russ. J. Coord. Chem.* **2020**, *46*, 411–419. [CrossRef]

44. Lutsenko, I.A.; Yambulatov, D.S.; Kiskin, M.A.; Nelyubina, Y.V.; Primakov, P.V.; Bekker, O.B.; Sidorov, A.A.; Eremenko, I.L. Mononuclear Cu(II), Zn(II), and Co(II) Complexes with 2-Furoate Anions and 2,2′-Bpy: Synthesis, Structure, and Biological Activity. *Russ. J. Coord. Chem.* **2020**, *46*, 787–794. [CrossRef]

45. Koshenskova, K.A.; Baravikov, D.E.; Nelyubina, Y.V.; Primakov, P.V.; Shender, V.O.; Maliyants, I.K.; Bekker, O.B.; Aliev, T.M.; Borodin, E.A.; Leusova, N.Y.; et al. Copper(II) Furancarboxylate Complexes with 5-Nitro-1,10-Phenanthroline as Promising Biological Agents. *Russ. J. Coord. Chem.* **2023**, *49*, 632–643. [CrossRef]

46. Dolomanov, O.V.; Bourhis, L.J.; Gildea, R.J.; Howard, J.A.K.; Puschmann, H. OLEX2: A Complete Structure Solution, Refinement and Analysis Program. *J. Appl. Crystallogr.* **2009**, *42*, 339–341. [CrossRef]

47. Sheldrick, G.M. A Short History of SHELX. *Acta Crystallogr. Sect. A* **2008**, *64*, 112–122. [CrossRef] [PubMed]
48. Sheldrick, G.M. Crystal Structure Refinement with SHELXL. *Acta Crystallogr. Sect. C* **2015**, *71*, 3–8. [CrossRef]
49. Ramón-García, S.; Ng, C.; Anderson, H.; Chao, J.D.; Zheng, X.; Pfeifer, T.; Av-Gay, Y.; Roberge, M.; Thompson, C.J. Synergistic Drug Combinations for Tuberculosis Therapy Identified by a Novel High-Throughput Screen. *Antimicrob. Agents Chemother.* **2011**, *55*, 3861–3869. [CrossRef]
50. Lyadova, I.V.; Eruslanov, E.B.; Khaidukov, S.V.; Yeremeev, V.V.; Majorov, K.B.; Pichugin, A.V.; Nikonenko, B.V.; Kondratieva, T.K.; Apt, A.S. Comparative Analysis of T Lymphocytes Recovered from the Lungs of Mice Genetically Susceptible, Resistant, and Hyperresistant to Mycobacterium Tuberculosis-Triggered Disease. *J. Immunol.* **2000**, *165*, 5921–5931. [CrossRef]
51. Majorov, K.B.; Nikonenko, B.V.; Ivanov, P.Y.; Telegina, L.N.; Apt, A.S.; Velezheva, V.S. Structural Modifications of 3-Triazeneindoles and Their Increased Activity Against Mycobacterium Tuberculosis. *Antibiotics* **2020**, *9*, 356. [CrossRef]
52. Alvarez, S. Distortion Pathways of Transition Metal Coordination Polyhedra Induced by Chelating Topology. *Chem. Rev.* **2015**, *115*, 13447–13483. [CrossRef]
53. Koshenskova, K.A.; Lutsenko, I.A.; Nebykov, D.N.; Mokhov, V.M.; Nelyubina, Y.V.; Primakov, P.V.; Popov, Y.V.; Khoroshilov, A.V.; Kottsov, S.Y.; Kiskin, M.A.; et al. Cu(II) Complexes as Catalyst Precursors in the Process of Selective Hydrogenation of Diene Hydrocarbons. *Polyhedron* **2023**, *230*, 116208. [CrossRef]
54. Nikiforova, M.E.; Lutsenko, I.A.; Kiskin, M.A.; Nelyubina, Y.V.; Primakov, P.V.; Bekker, O.B.; Khoroshilov, A.V.; Eremenko, I.L. Coordination Polymer of Ba^{2+} with 2-Furoic Acid Anions: Synthesis, Structure, and Thermal Properties. *Russ. J. Inorg. Chem.* **2021**, *66*, 1343–1349. [CrossRef]
55. Bekker, O.B.; Sokolov, D.N.; Luzina, O.A.; Komarova, N.I.; Gatilov, Y.V.; Andreevskaya, S.N.; Smirnova, T.G.; Maslov, D.A.; Chernousova, L.N.; Salakhutdinov, N.F.; et al. Synthesis and Activity of (+)-Usnic Acid and (−)-Usnic Acid Derivatives Containing 1,3-Thiazole Cycle against Mycobacterium Tuberculosis. *Med. Chem. Res.* **2015**, *24*, 2926–2938. [CrossRef]
56. Koshenskova, K.A.; Lutsenko, I.A.; Nelyubina, Y.V.; Primakov, P.V.; Aliev, T.M.; Bekker, O.B.; Khoroshilov, A.V.; Mantrov, S.N.; Kiskin, M.A.; Eremenko, I.L. Copper(II) Complexes with 5-Nitro-2-Furoic Acid: Synthesis, Structure, Thermal Properties, and Biological Activity. *Russ. J. Inorg. Chem.* **2022**, *67*, 1545–1556. [CrossRef]
57. Lutsenko, I.A.; Baravikov, D.E.; Koshenskova, K.A.; Kiskin, M.A.; Nelyubina, Y.V.; Primakov, P.V.; Voronina, Y.K.; Garaeva, V.V.; Aleshin, D.A.; Aliev, T.M.; et al. What Are the Prospects for Using Complexes of Copper(Ii) and Zinc(Ii) to Suppress the Vital Activity of Mycolicibacterium Smegmatis? *RSC Adv.* **2022**, *12*, 5173–5183. [CrossRef]